Journal of Alloys and Compounds 723 (2017) 75–83

Contents lists available at ScienceDirect

Journal of Alloys and Compounds

journal homepage: http://www.elsevier.com/locate/jalcom

Highly improved field emission from vertical graphene–carbon nanotube composites

Jian-Hua Deng [a, b, *], Rui-Nan Liu [a], Yan Zhang [a], Wen-Xiang Zhu [a], A-Long Han [a], Guo-An Cheng [c]

[a] College of Physics and Materials Science, Tianjin Normal University, Tianjin 300387, China
[b] Tianjin International Joint Research Centre of Surface Technology for Energy Storage Materials, Tianjin Normal University, Tianjin 300387, China
[c] Key Laboratory of Beam Technology and Material Modification of Ministry of Education, Beijing Normal University, Beijing 100875, China

ARTICLE INFO

Article history:
Received 5 April 2017
Received in revised form
13 June 2017
Accepted 24 June 2017
Available online 27 June 2017

Keywords:
Nanostructured materials
Vapor deposition
Electronic properties
Scanning electron microscopy
Transmission electron microscopy

ABSTRACT

Few-layer vertical graphene (VG) was prepared on arrayed carbon nanotubes (CNTs) without a catalyst by using radio frequency sputtering deposition and microwave plasma enhanced chemical vapor deposition, and the field emission (FE) performance of VG–CNT composites was tested and optimized. The FE performance is found to be strongly dependent on the heights (but not the actual heights) and densities of CNTs, the shapes of VG, and the diameters of VG–CNT composites. The optimal shapes for FE are demonstrated to be CNTs with middle densities and small diameters and VG with high densities and small sizes. The optimal FE performance from our large area VG–CNT composites is found to have a low threshold field of 1.28 V/μm (at 10 mA/cm^2), a high maximum emission current density of 87.63 mA/cm^2 (4.28 times higher than that from our previously prepared graphene–CNT composites), and excellent stability at an extremely high mean emission current density of 36.28 mA/cm^2 over a period of 50 h, far better than those of pristine CNTs, pure VG, and shape non-optimized VG–CNT composites.

1. Introduction

Graphene has proved to drastically influence the futuristic technology and even our daily lives due to its fascinating thermal, electrical, and mechanical properties [1–4]. It has aroused intensive interest in many applications such as energy storage [5], field effect transistors [6], and memory devices [7]. Graphene has also been demonstrated as a highly efficient field emission (FE) cathode material and the FE performance from single-, few-, and multi-layer graphene has been well reported over the last few years [8–11]. The sharp edge of graphene could serve as high-efficiency emission sites during FE and its unique two-dimensional surface is advantageous for faster heat dispersion and could greatly weaken Joule heating induced FE degradation [12]. In comparison with carbon nanotubes (CNTs), which have been demonstrated as an excellent FE cathode material in the past two decades [13–16], however, pure graphene emitters usually have higher operation voltages and lower current densities. This has aroused a need for the preparation of graphene–CNT composites, which are expected to have both the low working voltage of CNTs and the excellent FE stability of graphene. Two types of graphene–CNT composites are reported. (1) Graphene is flat-lying serving as a substrate for loading CNT emitters [17–19], but the FE capability from the sharp-edged graphene in this regime is totally buried. (2) Aligned CNTs are used as a substrate for growing vertical graphene (VG), which could fit our needs readily. As an example, Nayak et al. fabricated highly protruded graphene wrapped CNTs and ascribed the improved FE properties to the combined advantages of high aspect ratio and protruded graphene layers [20]. Kaushik et al. prepared graphene–CNT hybrids by using microwave plasma enhanced chemical vapor deposition (PECVD) and the hybrids were found to have a high field enhancement factor of ~6500 [21]. We also prepared VG on CNTs by using radio frequency (rf) sputtering deposition and microwave PECVD [22–24]. The FE performance of VG–CNT composites was found to outperform that of bare CNTs and VG. However, the VG–CNT composites we prepared have relatively low maximum emission current densities (J_{max}) [20–22] and poor FE stability at high current densities [24], and the underlying relationship between the FE response of emitters and the geometry of CNTs and VG needs to be further understood, which is

* Corresponding author. College of Physics and Materials Science, Tianjin Normal University, Tianjin 300387, China.
E-mail address: jhdeng1983@163.com (J.-H. Deng).

http://dx.doi.org/10.1016/j.jallcom.2017.06.280
0925-8388/

helpful for optimizing the morphology of VG–CNT emitters and achieving highly efficient field electron emission.

Here, we adopted rf sputtering deposition and microwave PECVD to prepare differently shaped VG–CNT composites and optimized their FE properties. The influence from the shapes of VG–CNT composites (CNT: height and density; VG: size and density; VG–CNT: diameter) on their FE performance is discussed. VG with high densities and small sizes, CNTs with good alignment and well-preserved tube-tube spaces, and VG–CNT composites with small diameters are demonstrated to be the optimal shapes for high-efficiency FE. The optimal FE performance is found to have a high J_{max} of 87.63 mA/cm^2 at 1.85 V/μm and excellent stability at a high mean emission current density (J_{mean}) of 36.28 mA/cm^2 over a period of 50 h, far better than those reported in previous studies [20–24].

2. Experimental details

2.1. Preparation of VG–CNT composites

The influence of experimental parameters (the concentration of carbon source, microwave power, and the growth time) on the growth of VG has been discussed in our previous studies [22,23]. Herein, we mainly discuss the influence of CNT shapes (heights and densities) on the FE performance of VG–CNT composites. The preparation of CNTs were performed on n-(100) Si wafers (resistivity: 1–10 Ω m; thickness: 505–545 μm; area: ~2 × 2 cm^2) by using the classical thermal CVD [22]. The Si wafers were pre-bombarded by iron ions at ~10 kV for 15 min using a metal vapor vacuum arc ion source followed by the deposition of a 5-nm-thick iron film as a catalyst using magnetron sputtering. The CNT growth was carried out in a tubular furnace under 600 sccm H_2 and 87 sccm C_2H_2 at 750 °C. The geometry of CNTs was controlled by changing the thickness of catalyst and the growth time. The resultant CNTs were further annealed at 1000 °C for 5 h. Both the iron ion pre-bombardment and the post-annealing are helpful for improving the adhesion of CNTs to substrates [24]. Microwave (2.45 GHz) PECVD and rf (13.56 MHz) sputtering deposition were employed to prepare the VG [22–24], and the VG shapes were mainly determined by changing the experimental methods. VG prepared by using microwave PECVD is densely distributed and has large sizes [23], while VG prepared by using rf sputtering is sparsely distributed and small-sized [22].

2.2. Structural characterizations

Scanning electron microscope (SEM, S–4800, Hitachi, Japan) was used to characterize the surface morphology of the as-received VG–CNT composites under an acceleration voltage of 10 kV. Their fine structure was observed by using a high-resolution transmission electron microscope (HRTEM, JEM–2010) operated at 200 kV. For TEM observation, the samples were prepared by following a process of scraping off from Si wafers, ultrasonicating in an ethanol bath for 15 min, and dropping the as-received solution onto a copper grid. Raman spectroscopy with a He–Ne laser (laser wavelength: 633 nm) was used to evaluate the perfection of our carbonaceous materials and roughly determine the number of layers of VG. The defect analysis was also performed by using X-ray photoelectron spectroscopy (XPS, PHI Quantera SXM) with Al Kα irradiation (~1486.6 eV).

2.3. FE measurements

FE measurements of the resultant VG–CNT composites were performed at room temperature by using a diode-type setup under an ultrahigh vacuum condition (~1.0 × 10^{-7} Pa), using our samples (sample area: ~2 × 2 mm^2) as the cathode against a stainless steel plate (~10 cm in diameter) as the anode. The surfaces of the cathode and anode were kept perfectly parallel to avoid inhomogeneous electric field. The cathode–anode gap was 1 mm. During FE tests, a DC bias voltage (0–10 kV) was applied to the anode at a constant rate of 500 V/min while grounding the cathode. The FE results were recorded in terms of emission current *versus* voltage by a computer.

3. Results and discussion

3.1. FE from VG–CNT composites with differently heighted CNTs

We first investigated the influence of CNT heights on the FE performance of VG–CNT composites. Fig. 1a–c shows side-view SEM images of CNTs with heights of 26, 17, and 10 μm, respectively. The height of CNTs was controlled by adjusting the growth time: 40, 25, and 15 min for the 26, 17, and 10 μm samples, respectively. All the CNTs are densely arrayed with their tips randomly distributed. VG was prepared on the CNTs by using rf sputtering deposition (parameters: 320 W, 300 Pa, 750 °C, 2.5 sccm H_2, and 10 h) and microwave PECVD (parameters: 100 W, 1 kPa, 800 °C, 4 sccm C_2H_2, 10 sccm H_2, and 4 h). The VG prepared by using rf sputtering is sparsely distributed on the top section of CNTs and is less than 200 nm in width (Fig. 1d), and the spaces among adjacent CNTs are well preserved (Fig. 1e). Upon the VG prepared by using PECVD, it reaches ~1 μm in width and is densely grown on CNTs forming a flower-like appearance (Fig. 1f), and the spaces among adjacent CNTs are fully filled by the large-size VG (Fig. 1g). This difference of the shapes of VG is mainly attributed to the fact that the concentration of carbon source in the rf system is much lower than that in the microwave PECVD system, resulting in that the VG grows much slower in the rf system [22,23]. Fig. 1h and i shows typical HRTEM images of these two types of VG–CNT composites and the insets are the corresponding TEM images. The VG prepared by using rf sputtering exhibits a folded edge of ~2 layers, while that for the VG prepared by using PECVD is ~10 layers.

Raman spectra analysis was performed in order to analyze the vibrational characteristics of our VG–CNT composites. Pure VG was prepared on Si wafers under the same growth conditions to eliminate the influence of CNTs on the Raman characterization of VG. Fig. 2a represents the Raman spectra of pure VG prepared by using rf sputtering and microwave PECVD. For both types of samples, two peaks corresponding to D band (~1327 cm^{-1}) and G band (~1575 cm^{-1}) appear [25]. The D band is sensitive to defects in graphitic structure, while the G band is associated with the E_{2g} vibration mode of graphitic carbon and is common in almost all kinds of graphitic materials [26,27]. The ratio of the intensity of the D band to G band (I_D/I_G) could be used as a measure to scale the defects in our carbon materials. The I_D/I_G values for the rf sputtering and microwave PECVD prepared VG are calculated to be 1.60 and 1.82, respectively, suggesting that (1) these two types of VG are rich in defects and (2) VG prepared by rf sputtering has more defects. The distinct peak centered at ~2643 cm^{-1} is the 2D peak, which arises from the two-phonon scattering process [28]. The ratio of the intensity of the 2D peak to G peak (I_{2D}/I_G) could be used to roughly evaluate the number of layers of graphene. For example, a single-layer graphene has an I_{2D}/I_G value up to ~4 [26]; few-layer (<10 layers) graphene has I_{2D}/I_G values approximate or larger than 1.00 [22,29]. The I_{2D}/I_G values for the rf sputtering and microwave PECVD prepared VG are calculated to be 1.61 and 1.00, respectively, indicating that all the VG is few-layer graphene and the VG prepared by using rf sputtering has less layers. The chemical bonding information of VG was further characterized by using XPS spectroscopy. Fig. 2b shows the C1s peak of the pure VG prepared by using rf sputtering and microwave PECVD. Peak

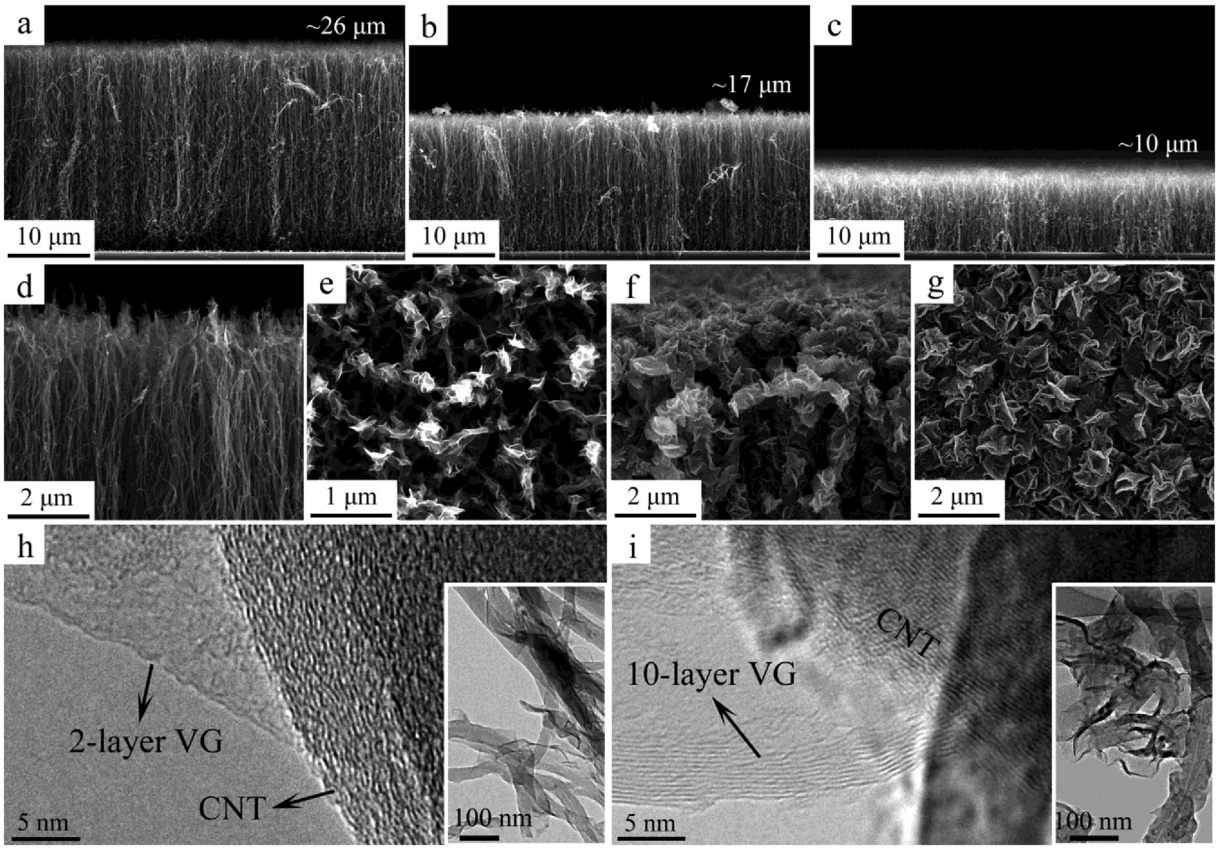

Fig. 1. Side-view SEM images of CNTs with heights of (a) 26, (b) 17, and (c) 10 μm. Typical (d,f) side- and (e,g) top-view SEM images of VG–CNT composites prepared by using (d,e) rf sputtering and (f,g) microwave PECVD. Typical HRTEM images of VG–CNT composites prepared by using (h) rf sputtering and (i) microwave PECVD, and the insets are the corresponding TEM images.

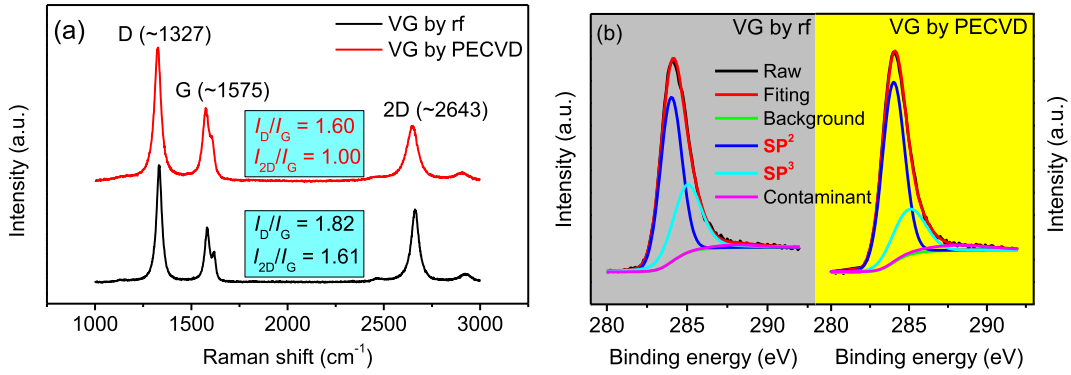

Fig. 2. (a) Raman and (b) XPS spectra of VG prepared on Si wafers by using rf sputtering deposition and microwave PECVD.

fitting of the C1s peak shows three component peaks centered at 284, 285, and 288 eV, which correspond with the SP^2- [30] and SP^3-hybridized carbon [31], and the oxygen contamination [32], respectively. The percentages of the SP^3-hybridized carbon for the VG prepared by using rf sputtering and microwave PECVD are 31.7% and 25.6%, respectively. Since defect-free graphitic materials are mainly constructed by SP^2-hybridized carbon, the presence of SP^3-hybridized carbon is related to the emergence of defects. This result indicates that the VG prepared by using rf sputtering has more defects, which is the same to the Raman results. These defects are mainly produced during the growth of VG and exist in the forms of vacancy-related defects such as protruding carbon atom, oxygen adatom, and hydrogen adatom [33], and are believed to be beneficial for improving the FE performance of emitters by means of introducing more active emission sites and providing more electron traces [34,35].

The FE performance of the as-received VG–CNT composites as well as pristine CNTs was estimated by using a parallel diode setup (middle inset of Fig. 3a). It is presented in terms of *J versus* applied field (*E*), *i.e.*, the FE *J*–*E* curves (Fig. 3a). Threshold electric field (E_{th}, *E* at 10 mA/cm^2), an important indicator in applications, is used to evaluate the FE capability of our samples (Fig. 3b). All the samples were first aged at ~10 mA/cm^2 under a constant *E* for 5 h to ensure that the FE *J*–*E* curve of each sample was obtained under a same condition [36,37]. The E_{th} for the 26 and 17 μm pristine CNTs is

subtly different (1.49 *versus* 1.51 V/μm), but it increases considerably to 1.63 V/μm for the 10 μm sample. Similar variation trend of the E_{th} is observed from the VG–CNT composites prepared by using rf sputtering deposition, *i.e.*, the 26 and 17 μm samples have similar E_{th} values while the 10 μm sample has a higher one. Optimal FE performance is obtained from the 26 μm rf sputtering prepared VG–CNT composites, with an ultralow E_{th} of 1.31 V/μm. This low E_{th} not only outperforms those of pristine CNTs but also is significantly superior to those reported for single- (5.20 V/μm) [8] and few-layer graphene (3.0 V/μm at 1.0 mA/cm^2) [9], and hybrid emitters such as graphene–Si nanowires (2.14 V/μm at 6.04 mA/cm^2) [29] and ZnO/Si nanotrees (2.18 V/μm at 10 μA/cm^2) [38]. Upon the PECVD prepared VG–CNT composites, it is interesting that the change of E_{th} is negligible: 1.74, 1.74, and 1.77 V/μm for the 26, 17, and 10 μm samples, respectively.

The Fowler–Nordheim (*F–N*) theory is the most-widely used model to understand the FE from the surface of a metal as well as nanostructures [7–10,22–24,39,40], which is also used to further understand the FE from our emitters. The work function of our samples was assumed to be the same as that of graphite (~5 eV) [8,9]. By taking the slope of the *F–N* curves ($\ln(J/E^2)$ *versus* $1/E$, inset of Fig. 3a) in the high-*E* regions, the field enhancement factor (β) of the samples could be determined, as plotted in Fig. 3b. The FE capability (corresponding with E_{th}) of the samples is found to be highly dependent on the β. For example, the 26 μm rf sputtering prepared VG–CNT composites, which have the best FE capability (Fig. 3a), is found to have the largest β (~6800); the differently heighted PECVD prepared VG–CNT composites, which have similar FE capability (Fig. 3a), is found to have similar β values (from 3335 to 3452). Comparison of the FE performance between pristine CNTs and rf sputtering prepared VG–CNT composites with the same height, the improved FE properties are ascribed to (1) the growth of vertical standing sharp edged VG and the introduction of defects [34,35] and wrinkles [41] on the surface of VG that increase the number of active emission sites and (2) the well preservation of the field enhancement from the high-aspect-ratio CNTs. Comparison of the FE performance between pristine CNTs and PECVD prepared VG–CNT composites with the same height, the considerably deteriorated FE performance after the growth of large-size VG is ascribed to the fact that the field enhancement from the high-aspect-ratio CNTs is highly shielded by the VG in this condition [23]. The above results indicate that the FE performance of VG–CNT composites is strongly dependent on the heights of CNTs and the shapes of VG. Although the β is an aspect ratio (h/d, where h and d are the height and diameter of an emitter) dependent parameter, this h is not the actual height of emitters due to the influence of field screening effect, which has been widely reported in densely distributed field emitters [42–44]. The β is a complicated factor also determined by some other parameters (which are hard to be quantitatively determined) such as the number of active emission sites of emitters and the radius of the tip of each emitter. Thus the underlying relationship between the geometry and the FE performance of emitters still requires better understanding and more efforts should be made in this respect in the future.

3.2. FE from VG–CNT composites with differently densed CNTs

The influence of the density of CNTs on the FE performance of VG–CNT composites is studied to further optimize their FE properties. Fig. 4a–c shows side-view SEM images of CNTs with different densities. The density of CNTs was controlled by adjusting the thickness of iron catalyst [22–24,45], which was 1, 5, and 15 nm for the growth of CNTs with high, middle, and low densities, respectively. It can be seen from the insets of Fig. 4a and b that the number of CNTs for the high- and middle-dense samples is ~30 and ~15 within 500 nm width, respectively, while for the low-sense sample is ~16 within 2 μm width (Fig. 4c). VG with sparse (Fig. 4d) and dense (Fig. 4e) distribution was prepared on the CNTs by using rf sputtering and microwave PECVD, respectively. The growth parameters for rf sputtering were 300 W, 300 Pa, 750 °C, 2.5 sccm H_2, and 10 h; for microwave PECVD were 100 W, 1 kPa, 800 °C, 4 sccm C_2H_2, 10 sccm H_2, and 4 h.

Fig. 5a shows the FE *J–E* curves of pristine CNTs, and differently densed VG–CNT composites prepared by using rf sputtering and microwave PECVD. H, M, and L in Fig. 5a represent CNTs with high, middle, and low densities. These curves were obtained after an aging process performed at ~10 mA/cm^2 for 5 h [36,37]. The E_{th} and β of the samples are plotted in Fig. 5b. For samples with same densities, it can be found that all the VG–CNT composites have better FE performance than that of bare CNTs, especially for the low-dense CNTs, whose J_{max} increases from 5.17 to more than 10 mA/cm^2 after the growth of VG on CNTs. The optimal FE performance is obtained from the middle-dense rf sputtering prepared VG–CNT composites. It has a low E_{th} of 1.29 V/μm and a high β of ~6917. According to our above discussions, this FE improvement is ascribed to the introduction of high-efficiency emission sites and also the highly preserved FE enhancement from the CNTs. For pristine CNTs and the rf sputtering prepared VG–CNT composites, the FE performance of the high-dense samples is found to be inferior to that of the middle-dense ones. This is ascribed to the fact

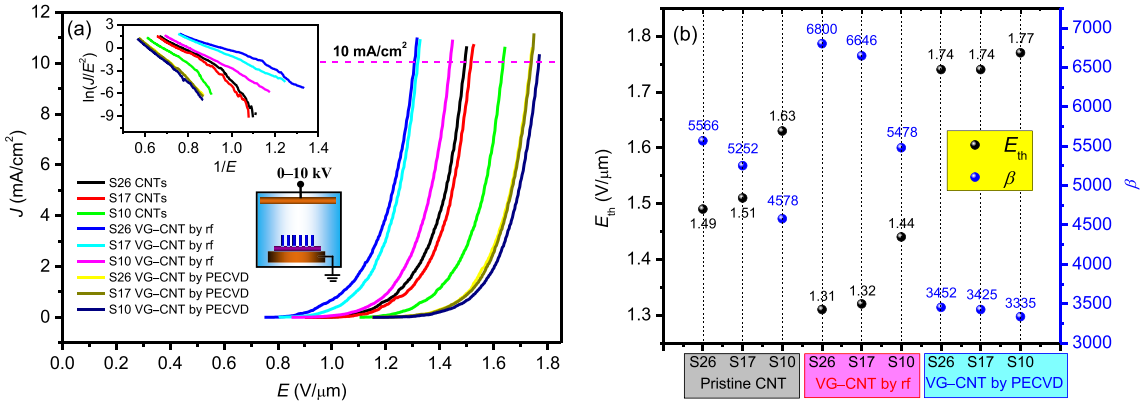

Fig. 3. (a) FE *J–E* curves of differently heighted pristine CNTs and VG–CNT composites prepared by using rf sputtering and microwave PECVD. Inset (upper): the corresponding *F–N* curves; inset (middle): schematic of the diode-type setup used for FE tests. (b) The E_{th} and field enhancement factor (β) of the samples. S26, S17, and S10 represent samples with CNT heights of 26, 17, and 10 μm, respectively.

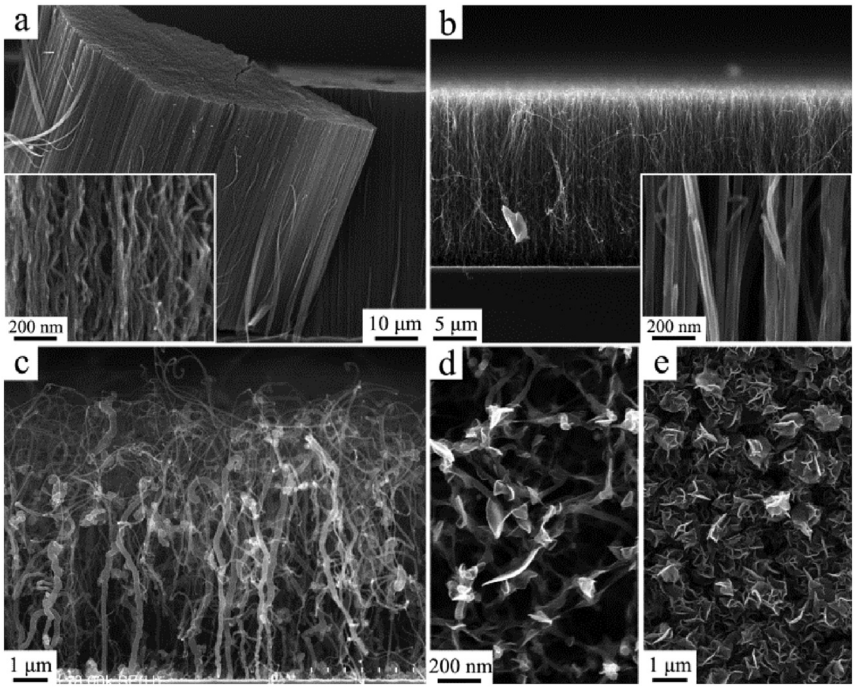

Fig. 4. Side-view SEM images of CNTs with (a) high, (b) middle, and (c) low densities. Typical top-view SEM images of VG–CNT composites prepared by using (d) rf sputtering and (e) microwave PECVD.

that the field screening in this high-dense condition is far stronger than that in the middle-dense condition [42–44]. For the PECVD prepared VG–CNT composites, the FE performance of the high-dense samples gets worse and even approaches that of VG prepared on Si wafers [29]. This is attributed to the fact that the tube-tube spaces for the high-dense CNTs are fully filled by the large-size VG, resulting in that the surface of the CNT arrays is similar to that of planar Si wafers, and the field enhancement from the CNTs is totally buried in this condition.

Excellent FE stability along with low operation fields are an attractive preposition for vacuum electron device applications. The FE stability (*J versus* time) of CNTs and VG–CNT composites with different densities was tested for comparison, as shown in Fig. 6. All the *J*–time curves were obtained at ~10 mA/cm^2 (for samples with a J_{max} higher than 10 mA/cm^2) or ~50% J_{max} (for samples with a J_{max} less than 10 mA/cm^2) and without aging. The FE stability is characterized by J_{drop}, which is calculated from $(J_{first} - J_{last})/J_{first}$, where J_{first} and J_{last} are the first and last recorded *J* during a stability test, respectively. Fig. 6a–c shows 60 min FE stability of these three types of samples and the corresponding J_{drop} values are shown in Table 1. Horizontal comparison of the J_{drop} shows that the high-dense samples, regardless of the growth of VG, have better FE stability than that of the middle- and low-dense ones. This is ascribed to the influence of field screening [42–44], which results in that the FE current from an individual CNT or VG–CNT for the low-dense samples is much higher than that for the high-dense ones. This is the most important reason that an individual CNT or a CNT bundle has an extremely high *J* up to several A/cm^2 [46,47], but FE from large-area (>1 mm^2) densely arrayed CNTs with a *J* higher than 50 mA/cm^2 is rarely reported. For these sparsely distributed CNTs with high currents, they are more likely to be destroyed by Joule heating and peeled off by the strong electrostatic force during FE [12,24,48], resulting in the deterioration of the FE performance of emitters. Vertical comparison of the J_{drop} shows

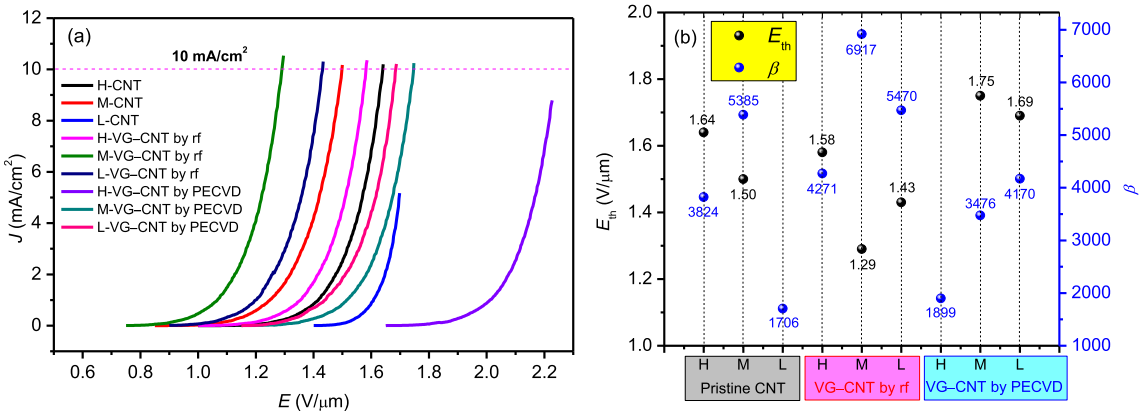

Fig. 5. (a) FE *J*–*E* curves of pristine CNTs and differently densed VG–CNT composites prepared by using rf sputtering and microwave PECVD. (b) E_{th} and field enhancement factor (β) of the samples. H, M, and L represent CNTs with high, middle, and low densities.

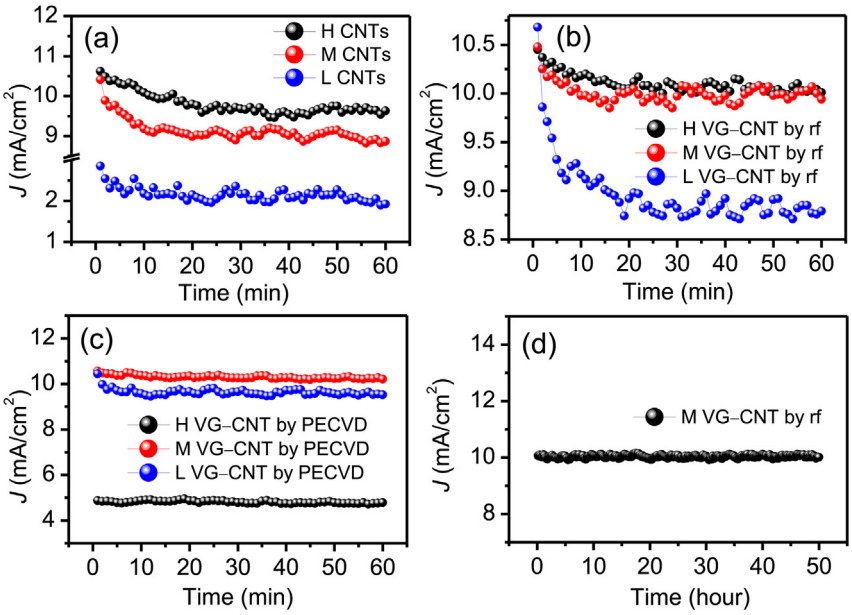

Fig. 6. 60 min FE stability of (a) pristine CNTs and differently densed VG–CNT composites prepared by using (b) rf sputtering and (c) microwave PECVD. (d) 50 h FE stability of the rf sputtering prepared middle-dense VG–CNT composites after being aged. H, M, and L represent CNTs with high, middle, and low densities.

that the growth of VG is helpful for improving the FE stability of CNT arrays. This is ascribed to the unique two-dimensional structure of VG that allows faster heat dispersion and thus weakens Joule heating induced decrease of active emission sites [12]. Fig. 6d shows the 50 h FE stability of the same rf sputtering prepared VG–CNT sample, and this *J*–time curve was obtained right after the 60 min test (Fig. 6b). It exhibits excellent FE stability, with an extremely small J_{drop} of 0.50% and negligible current fluctuations: <1.2% with respect to the J_{mean}. The above results indicate that a sparse distribution of emitters benefits the concentration of high local applied fields at emission sites but it is detrimental to FE for lack of enough active emission sites, especially for applications calling for high-*J* and longtime stable electron emission.

3.3. FE performance of VG–CNT composites with different diameters

The influence of the diameters of VG–CNT composites on their FE performance is further studied. Fig. 7a and b shows side-view SEM images of microwave PECVD prepared thin (50–60 nm in diameters) and thick (~100 nm in diameters) VG–CNT composites, respectively. The key growth parameter was the gas flow of C_2H_2 during the growth of VG, which was 3.5 and 7 sccm for the preparation of the thin and thick samples, respectively (other growth conditions were 1 kPa, 150 W, 750 °C, 10 sccm H_2, and 3 h). The thickening of VG–CNT composites is ascribed to the high concentration of carbon source induced quick deposition of carbon atoms [23]. Instead of diffusing on the surface of CNTs and forming covalent bonds at the edges of VG, which leads to the two-dimensional growth of VG and the growth mechanism has been well addressed previously [49–51], these quickly deposited carbon atoms are bonded by means of forming amorphous carbon, resulting in the increase of VG–CNT diameters. For the thin VG–CNT composites, small-sized VG is densely grown on the surface of CNTs and in particular, the spaces among adjacent CNTs are well preserved. Upon the thick ones, the CNTs thicken significantly with only small tube-tube spaces left.

Table 1
The J_{drop} of pristine CNTs and differently densed VG–CNT composites in the 60 min FE stability tests.

J_{drop} (%)	High-dense	Middle-dense	Low-dense
CNTs	9.32	14.79	32.63
VG–CNT by rf	4.21	5.15	17.70
VG–CNT by PECVD	1.85	3.31	8.81

Fig. 7c shows the FE *J*–*E* performance of the thin and thick VG–CNT composites obtained after being aged at ~10 mA/cm^2 for 5 h. The E_{th} and β for the thin and thick samples are 1.28 *versus* 1.86 V/μm and 8219 *versus* 3355, respectively. Fig. 7d shows the FE *J*–*E* curves of these two types of samples obtained until the *J* reaches the J_{max}. The J_{max} for the thin VG–CNT composites is up to 87.63 mA/cm^2 at 1.85 V/μm, much higher than 29.72 mA/cm^2 at 2.02 V/μm for the thick ones. These FE results from the thin VG–CNT composites also outperform those obtained from dense CNT based emitters reported in previous studies. The E_{th} is far smaller than the values (>2.0 V/μm) reported previously [8,9,29,38]; the J_{max} is 4.28 times higher than that of the few-layer graphene–CNT composites reported in our previous study (~20.47 mA/cm^2) [22]. This improved FE performance is ascribed to the good preservation of spaces among adjacent CNTs. Comparison of the E_{th} shown in Fig. 7c and d, the increase of E_{th} for the same sample is ascribed to the circular tests induced aging of our emitters, which has been discussed in detail in our previous study [24]. Fig. 7e shows the 300 s FE stability of these two types of samples at J = ~10 mA/cm^2, with the FE data recoded in every 5 s and without any aging process, which is helpful for comparing the initial uniformity of FE currents. The J_{drop} values for the thin and thick VG–CNT composites are 2.82% and 0.39%, respectively, and the current fluctuations for the thin sample are more intense. Similar FE stability trend was observed at J = ~50% J_{max} over a period of 20 h: the J_{drop} for the thin and thick samples are 7.45% and 2.79%, respectively, with the FE data recoded in every 10 min and without any aging process, as shown in Fig. 7f. The results indicate that the VG–CNT composites with thickened CNTs, which have poorer FE capability (Fig. 7c and d), have better FE stability. This is attributed to the reinforcement from the coated amorphous carbon layer on the surface of CNTs. This layer makes our thickened CNTs more difficult to be destroyed by the Joule heat

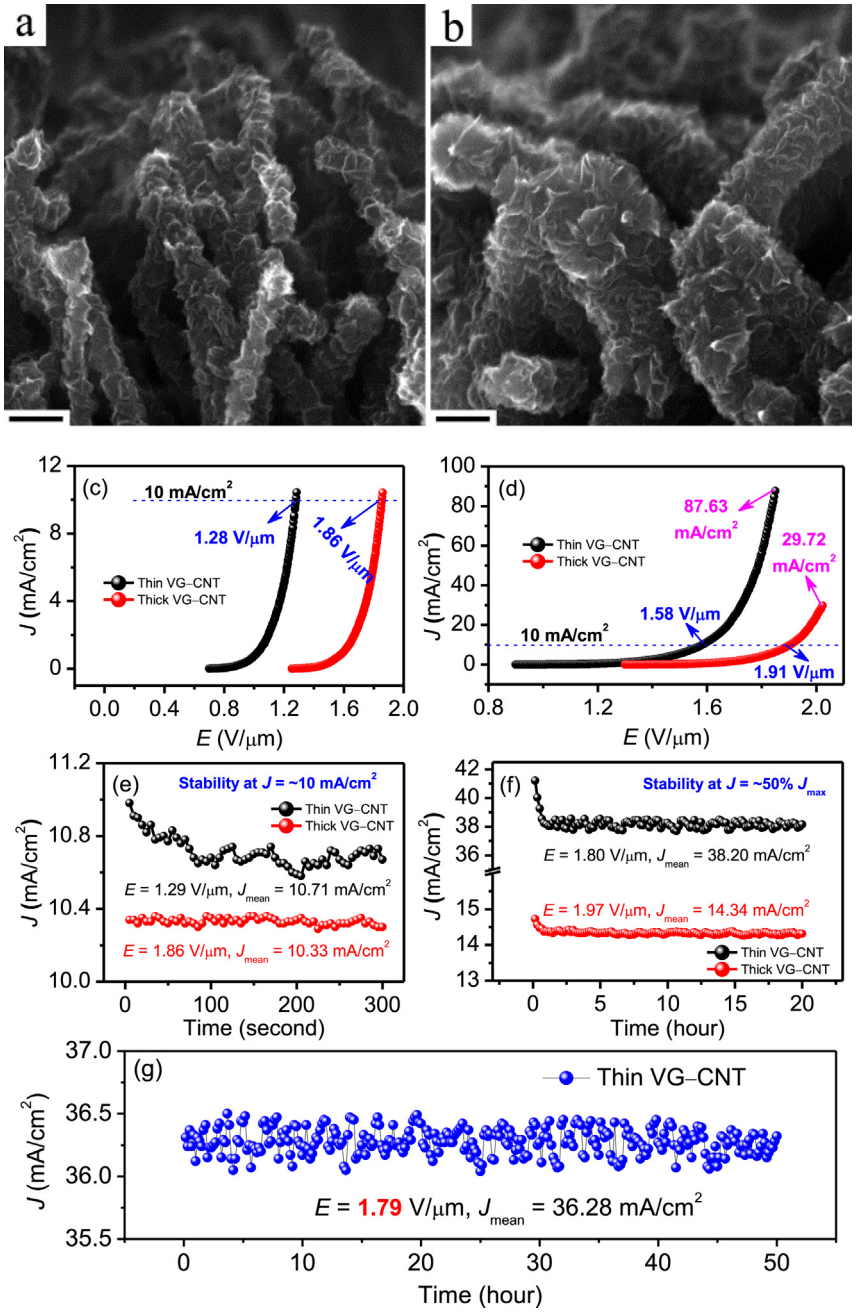

Fig. 7. Side-view SEM images of (a) thin and (b) thick VG–CNT composites. All the scale bars are 100 nm. FE J–E curves of these two types of composites obtained (c) right after being aged at ~10 mA/cm^2 for 5 h and (d) until the J achieves the J_{max}. FE stability of these two types of composites at (e) J = ~10 mA/cm^2 for 300 s and (f) J = ~50% J_{max} for 20 h. (g) 50 h FE stability of the same thin VG–CNT composites after slightly decreasing the constant E from 1.80 to 1.79 V/μm.

during high-current FE as compared with pristine or slightly thickened CNTs [12,52]. Although the thick VG–CNT composites have better FE stability, the thin ones have much lower E and higher J, and their FE current becomes stable after the first 1 h test. Fig. 7g shows 50 h FE stability of the same thin VG–CNT composites after slightly decreasing the constant E from 1.80 to 1.79 V/μm. It can be seen that our emitters show excellent FE stability at an extremely high J_{mean} of 36.28 mA/cm^2 and the FE current is almost stable with negligible fluctuations (<0.6% with respect to the J_{mean}). Considering the large area (~2 × 2 mm^2) and the dense distribution of our samples, this FE stability is excellent. It is far better than the FE stability of CNT or VG based emitters reported previously [8,9,14,19,22–24,29]. The CNTs [14], VG [29], and graphene–CNT composites [22–24] we reported previously could only work at J_{mean} < 20 mA/cm^2 (usually at J_{mean} = ~10 mA/cm^2). This improved FE stability at 1.79 V/μm is ascribed to the deep aging of our samples after the 20 h stability test at 1.80 V/μm [36,37]. The above results indicate that both the growth of densely distributed and small-sized VG (brings sufficient active emission sites to emitters) and the good preservation of spaces among adjacent CNTs (leads to easy concentration of high local applied fields at emission sites) are important for achieving high-performance (low-E, high-J, and longtime stable FE) field electron emission.

4. Conclusions

Differently shaped VG was prepared on differently shaped CNTs by using rf sputtering deposition and microwave PECVD, and the FE

performance of VG–CNT composites was studied and optimized. Structural analyses indicate that the VG is typical few-layer graphene rich in defects and the VG prepared by using rf sputtering is thinner than that prepared by using microwave PECVD. The FE performance of VG–CNT composites is found to be strongly dependent on the heights (but not the actual heights) and densities of CNTs, the shapes of VG, and the diameters of VG–CNT composites. The rf sputtering prepared VG–CNT composites with small-sized VG and not thickened CNTs are found to have far better FE capability than that of bare CNTs due to the considerable increase of high-efficiency emission sites and also the good preservation of the field enhancement from the high-aspect-ratio CNTs. The PECVD prepared VG–CNT composites with large-sized VG and thickened CNTs are found to have poor FE performance mainly due to the shielding of the field from the CNTs. The optimal shapes for FE are VG with small sizes and high densities and CNTs with middle densities and small diameters. The FE performance obtained from the VG–CNT composites with optimal shapes shows a low E_{th} of 1.28 V/μm, a high J_{max} of 87.63 mA/cm^2, and excellent FE stability at an extremely high J_{mean} of 36.28 mA/cm^2 under 1.79 V/μm over a period of 50 h. These results have shed light on applications calling for low operation voltages, high currents, and longtime stable field electron emission.

Acknowledgements

This work was supported by the Key Project of Tianjin Natural Science Foundation (14JCZDJC32100) and the National Natural Science Foundation of China for Youth Science Funds (51302187).

References

[1] K.S. Novoselov, A.K. Geim, S.V. Morozov, D. Jiang, Y. Zhang, S.V. Dubonos, I.V. Grigorieva, A.A. Firsov, Electric field effect in atomically thin carbon films, Science 306 (2004) 666–669.
[2] K.S. Novoselov, Z. Jiang, Y. Zhang, S.V. Morozov, H.L. Stormer, U. Zeitler, J.C. Maan, G.S. Boebinger, P. Kim, A.K. Geim, Room-temperature quantum Hall effect in graphene, Science 315 (2007) 1379.
[3] C. Si, W.H. Duan, Z. Liu, F. Liu, Electronic strengthening of graphene by charge doping, Phys. Rev. Lett. 109 (2012) 226802.
[4] T. Low, P. Avouris, Graphene plasmonics for terahertz to mid-infrared applications, ACS Nano 8 (2017) 1086–1101.
[5] J.L. Yang, J.J. Wang, Y.J. Tang, D.N. Wang, X.F. Li, Y.H. Hu, R.Y. Li, G.X. Liang, T.K. Sham, X.L. Sun, $LiFePO_4$–graphene as a superior cathode material for rechargeable lithium batteries: impact of stacked graphene and unfolded graphene, Energy Environ. Sci. 6 (2013) 1521–1528.
[6] F. Khan, S.H. Baek, J.H. Kim, One-step and controllable bipolar doping of reduced graphene oxide using TMAH as reducing agent and doping source for field effect transistors, Carbon 100 (2016) 608–616.
[7] Z.X. Wang, S. Eigler, Y. Ishii, Y.C. Hu, C. Papp, O. Lytken, H.P. Steinrück, M. Halik, A facile approach to synthesize an oxo-functionalized graphene/polymer composite for low-voltage operating memory devices, J. Mater. Chem. C 3 (2015) 8595–8604.
[8] Z.S. Wu, S.F. Pei, W.C. Ren, D.M. Tang, L.B. Gao, B.L. Liu, F. Li, C. Liu, H.M. Cheng, Field emission of single-layer graphene films prepared by electrophoretic deposition, Adv. Mater. 21 (2009) 1756–1760.
[9] L.L. Jiang, T.Z. Yang, F. Liu, J. Dong, Z.H. Yao, C.M. Shen, S.Z. Deng, N.S. Xu, Y.Q. Liu, H.J. Gao, Controlled synthesis of large-scale, uniform, vertically standing graphene for high-performance field emitters, Adv. Mater. 25 (2013) 250–255.
[10] C.X. Zhao, Y. Zhang, S.Z. Deng, N.S. Xu, J. Chen, Surface nitrogen functionality for the enhanced field emission of free-standing few-layer graphene nanowalls, J. Alloys Compd. 672 (2016) 433–439.
[11] A. Kumar, S. Khan, M. Zulfequar, M. Husain, Low temperature synthesis and field emission characteristics of single to few layered graphene grown using PECVD, Appl. Surf. Sci. 402 (2017) 161–167.
[12] K.A. Dean, T.P. Burgin, B.R. Chalamala, Evaporation of carbon nanotubes during electron field emission, Appl. Phys. Lett. 79 (2001) 1873–1875.
[13] A. Kumar, S. Parveen, S. Husain, M. Zulfequar, M. Husain, Oxygen and nitrogen doping in single wall carbon nanotubes: an efficient stable field emitter, J. Alloys Compd. 711 (2017) 85–93.
[14] J.H. Deng, X.G. Hou, L. Cheng, F.J. Wang, B. Yu, G.Z. Li, D.J. Li, G.A. Cheng, S.L. Wu, Irradiation damage determined field emission of ion irradiated carbon nanotubes, ACS Appl. Mater. Interfaces 6 (2014) 5137–5143.
[15] A. Pandey, A. Prasad, J.P. Moscatello, M. Engelhard, C.M. Wang, Y.K. Yap, Very stable electron field emission from strontium titanate coated carbon nanotube matrices with low emission thresholds, ACS Nano 7 (2013) 117–125.
[16] V.J. Scott, H. Manohara, R. Toda, L. Del Castillo, R. Murthy, J. Mulder, E. Murty, M.C. Thompson, Robust CNT field emitters: patterning, growth, transfer, and in situ anchoring, Nanotechnology 27 (2016) 494002.
[17] D.D. Nquyen, N.H. Tai, S.Y. Chen, Y.L. Chueh, Controlled growth of carbon nanotube–graphene hybrid materials for flexible and transparent conductors and electron field emitters, Nanoscale 4 (2012) 632–638.
[18] D.H. Lee, J.A. Lee, W.J. Lee, S.O. Kim, Flexible field emission of nitrogen-doped carbon nanotubes/reduced graphene hybrid films, Small 7 (2011) 95–100.
[19] R. Kumar, R.K. Singh, D.P. Singh, A.R. Vaz, R.R. Yadav, C.S. Rout, S.A. Moshkalev, Synthesis of self-assembled and hierarchical palladium-CNTs-reduced graphene oxide composites for enhanced field emission properties, Mater. Des. 122 (2017) 110–117.
[20] P. Nayak, P.N. Santhosh, S. Ramaprabhu, Enhanced electron field emission of one-dimensional highly protruded graphene wrapped carbon nanotube composites, J. Phys. Chem. C 118 (2014) 5172–5179.
[21] V. Kaushik, A.K. Shukla, V.D. Vankar, Microwave plasma CVD-grown graphene-CNT hybrids for enhanced electron field emission applications, Appl. Phys. A 117 (2017) 2197–2205.
[22] J.H. Deng, R.T. Zheng, Y. Zhao, G.A. Cheng, Vapor–solid growth of few-layer graphene using radio frequency sputtering deposition and its application on field emission, ACS Nano 6 (2012) 3727–3733.
[23] J.H. Deng, G.A. Cheng, R.T. Zheng, B. Yu, G.Z. Li, X.G. Hou, M.L. Zhao, D.J. Li, Catalyst-free, self-assembly, and controllable synthesis of graphene flake–carbon nanotube composites for high-performance field emission, Carbon 67 (2014) 525–533.
[24] J.H. Deng, L. Cheng, F.J. Wang, G.Z. Li, D.J. Li, G.A. Cheng, High current density and longtime stable field electron transfer from large-area densely arrayed graphene nanosheet–carbon nanotube hybrids, ACS Appl. Mater. Interfaces 6 (2014) 21558–21566.
[25] Z.S. Wu, W. Ren, L. Gao, J. Zhao, Z. Chen, B. Liu, D. Tang, B. Yu, C. Jiang, H. Cheng, Synthesis of graphene sheets with high electrical conductivity and good thermal stability by hydrogen arc discharge exfoliation, ACS Nano 3 (2009) 411–417.
[26] A.C. Ferrari, J.C. Meyer, V. Scardaci, C. Casiraghi, M. Lazzeri, F. Mauri, S. Piscanec, D. Jiang, K.S. Novoselov, S. Roth, A.K. Geim, Raman spectrum of graphene and graphene layers, Phys. Rev. Lett. 97 (2006) 197401.
[27] K.N. Kudin, B. Ozbas, H.C. Schniepp, R.K. Prud'Homme, I.A. Aksay, R. Car, Raman spectra of graphite oxide and functionalized graphene sheets, Nano Lett. 8 (2008) 36–41.
[28] S. Sahoo, G. Khurana, S.K. Barik, S. Dussan, D. Barrionuevo, R.S. Katiyar, In situ Raman studies of electrically reduced graphene oxide and its field-emission properties, J. Phys. Chem. C 117 (2013) 5485–5491.
[29] F.J. Wang, L.N. Deng, J.H. Deng, Facile synthesis of differently shaped, ultrathin, and aligned graphene flakes without a catalyst for highly efficient field emission, Appl. Surf. Sci. 355 (2015) 218–225.
[30] R. Bertoncello, A. Casagrande, M. Casarin, A. Glisenti, E. Lanzoni, L. Mirenghi, E. Tondello, Tin, Tic and Ti (C, N) film characterization and its relationship to tribological behaviour, Surf. Interface Anal. 18 (1992) 525–531.
[31] P. Sundberg, R. Larsson, B. Folkesson, On the core electron binding energy of carbon and the effective charge of the carbon atom, J. Electron Spectrosc. Relat. Phenom. 46 (1988) 19–29.
[32] D. Rats, L. Vandenbulcke, R. Herbin, R. Benoit, R. Erre, V. Serin, J. Sevely, Characterization of diamond films deposited on titanium and its alloys, Thin Solid Films 270 (1995) 177–183.
[33] C. Kim, K. Seo, B. Kim, N. Park, Y.S. Choi, K.A. Park, Y.H. Lee, Tip-functionalized carbon nanotubes under electric fields, Phys. Rev. B 68 (2003) 115403.
[34] G. Wei, Emission property of carbon nanotube with defects, Appl. Phys. Lett. 89 (2006) 143111.
[35] G. Kim, B.W. Jeong, J. Ihm, Deep levels in the band gap of the carbon nanotube with vacancy-related defects, Appl. Phys. Lett. 88 (2006) 193107.
[36] H.S. Jang, S.K. Jeon, S.H. Nahm, Field emission properties from the tip and side of multi-walled carbon nanotube yarns, Carbon 48 (2010) 4019–4023.
[37] H.J. Jeong, H.D. Jeong, H.Y. Kim, J.S. Kim, S.Y. Jeong, J.T. Han, D.S. Bang, G.W. Lee, All-carbon nanotube-based flexible field-emission devices: from cathode to anode, Adv. Funct. Mater. 21 (2011) 1526–1532.
[38] S.S. Lv, Z.C. Li, C.H. Chen, J.C. Liao, G.J. Wang, M.Y. Li, W. Miao, Enhanced field emission performance of hierarchical ZnO/Si nanotrees with spatially branched heteroassemblies, ACS Appl. Mater. Interfaces 7 (2015) 13564–13568.
[39] F. Liu, J.F. Tian, L.H. Bao, T.Z. Yang, C.M. Shen, X.Y. Lai, Z.M. Xiao, W.G. Xie, S.Z. Deng, J. Chen, J.C. She, N.S. Xu, H.J. Gao, Fabrication of vertically aligned single-crystalline boron nanowire arrays and investigation of their field-emission behaviour, Adv. Mater 20 (2008) 2609–2615.
[40] S.S. Fan, M.G. Chapline, N.R. Franklin, T.W. Tombler, A.M. Cassell, H.J. Dai, Self-oriented regular arrays of carbon nanotubes and their field emission properties, Science 283 (1999) 512–514.
[41] Y.F. Guo, W.L. Guo, Electronic and field emission properties of wrinkled graphene, J. Phys. Chem. C 117 (2013) 692–696.
[42] J.S. Suh, K.S. Jeong, J.S. Lee, I. Han, Study of the field-screening effect of highly ordered carbon nanotube arrays, Appl. Phys. Lett. 80 (2002) 2392–2394.
[43] C. Li, Y. Yang, X.W. Sun, W. Lei, X.B. Zhang, B.P. Wang, J.X. Wang, B.K. Tay, J.D. Ye, G.Q. Lo, D.L. Kwong, Enhanced field emission from injector-like ZnO nanostructures with minimized screening effect, Nanotechnology 18 (2007)

135604.
[44] L. Wang, F. Gao, S. Chen, C. Li, W. Yang, Nanowire-density-dependent field emission of n-type 3C-SiC nanoarrays, Appl. Phys. Lett. 107 (2015) 122108.
[45] H.P. Liu, G.A. Cheng, Y. Zhao, R.T. Zheng, C.L. Liang, F. Zhao, T.H. Zhang, Controlled growth of Fe catalyst film for synthesis of vertically aligned carbon nanotubes by glancing angle deposition, Surf. Coat. Technol. 201 (2006) 938–942.
[46] Z. Xu, X.D. Bai, E.G. Wang, Z.L. Wang, Field emission of individual carbon nanotube with in situ tip image and real work function, Appl. Phys. Lett. 87 (2005) 163106.
[47] S. Fujii, S. Honda, H. Machida, H. Kawai, K. Ishida, M. Katayama, H. Ruruta, T. Hirao, K. Oura, Efficient field emission from an individual aligned carbon nanotube bundle enhanced by edge effect, Appl. Phys. Lett. 90 (2007) 153108.
[48] J.T.L. Thong, C.H. Oon, W.K. Eng, W.D. Zhang, L.M. Gan, High-current field emission from a vertically aligned carbon nanotube field emitter array, Appl. Phys. Lett. 79 (2001) 2811–2813.
[49] Y.H. Lee, S.G. Kim, D. Tománek, Catalytic growth of single-wall carbon nanotubes: an ab initio study, Phys. Rev. Lett. 78 (1997) 2393–2396.
[50] O.A. Louchev, Y. Sato, H. Kanda, Growth mechanism of carbon nanotube forests by chemical vapor deposition, Appl. Phys. Lett. 80 (2002) 2752–2754.
[51] M.Y. Zhu, J.J. Wang, B.C. Holloway, R.A. Outlaw, X. Zhao, K. Hou, V. Shutthanandan, D.M. Manos, A mechanism for carbon nanosheet formation, Carbon 45 (2007) 2229–2234.
[52] S.H. Jo, Y. Tu, Z.P. Huang, D.L. Carnahan, J.Y. Huang, D.Z. Wang, Z.F. Ren, Correlation of field emission and surface microstructure of vertically aligned carbon nanotubes, Appl. Phys. Lett. 84 (2004) 413–415.